THE JOURNAL OF PHYSICAL CHEMISTRY C

Article

Cite This: J. Phys. Chem. C 2019, 123, 3309−3320

pubs.acs.org/JPCC

Electronic Structure and Optical Properties of Designed Photo-Efficient Indoline-Based Dye-Sensitizers with D−A−π−A Framework

Juganta K. Roy, Supratik Kar, and Jerzy Leszczynski*

Interdisciplinary Center for Nanotoxicity, Department of Chemistry, Physics and Atmospheric Sciences, Jackson State University, Jackson, Mississippi 39217, United States

Supporting Information

ABSTRACT: Seven D−A−π−A-based indoline (IND) dyes that were designed via quantitative-structure−property relationship modeling have been comprehensively investigated using computational approaches to evaluate their prospect of application in future dye-sensitized solar cells (DSSCs). An array of optoelectronic properties of the isolated dye and dyes adsorbed on a TiO_2 cluster that simulates the semiconductor were explored by density functional theory (DFT) and time-dependent DFT methods. Light absorption spectra, vertical dipole moment, shift of the conduction band of semiconductor, excited state lifetime, driving force of electron injection, photostability of the excited state, and exciton binding energy were computed. Our study showed that the presence of an internal acceptor such as pyrido[3,4-*b*]pyrazine (pyrazine) would influence greater the open circuit voltage (V_{OC}), compared to the benzothiadiazole moiety. Considering the balance between the V_{OC} and J_{SC} (short circuit current) along with the all calculated characteristics, the IND3, IND5, and IND10 are the most suited among the designed dyes to be used as potential candidates for the photo-efficient DSSCs. The present study provides the results of rational molecular design followed by exploration of photophysical properties to be used as a valuable reference for the synthesis of photo-efficient dyes for DSSCs.

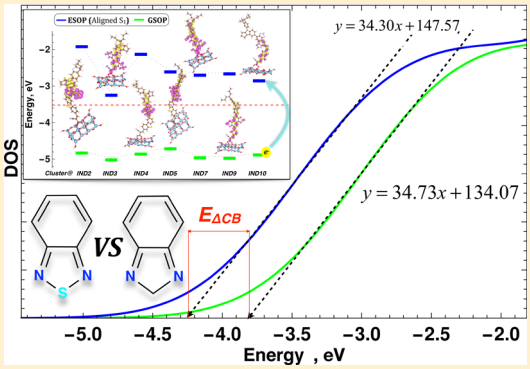

INTRODUCTION

Environment-friendly and renewable energy systems have drawn more attention nowadays due to increasing clean energy demands in "Generation Y". A number of research efforts have garnered to understand the processes of converting and storing solar energy in a specific molecular system.[1−5] Dye-sensitized solar cells (DSSCs) have been explored comprehensively as impending contenders for the solar renewable-energy device/systems. This is due to their reasonable efficiency, flexible structural modifications, high molar extinction coefficients, and low cost, compared to their counterpart ruthenium complex inorganic dyes.[6,7] The performance of any DSSCs system essentially depends on several factors: (1) solar light absorption efficiency by the sensitizing dye; (2) efficient charge separation which signifies uninterrupted transfer of electrons from the excited sensitizing dye to TiO_2; and (3) possibility of transfer of electron from the electron donor to the oxidized dye.[2] Most of these factors are meticulously concomitant with the structure of the sensitizing dye in ground and excited electronic states.[8] Thus, it is imperious to examine the electronic structures of the sensitizing dye molecule for the understanding of the mechanism of the charge separation and electron transfers. Such study could be then followed by designing and synthesizing of more efficient sensitizing dyes with enhanced power conversion efficiency (PCE).[9,10]

Organic dyes are primarily designed based on a D−π−A structure framework, where D and A stand for donor and acceptor fragments and π is the conjugated linker between D and A. The D−π−A structure represents well-established high-performance organic sensitizers because of their synthetic accessibility and ability to facilitate the intramolecular charge transfer (ICT) upon excitation.[11] To red-shift the ICT band of D−π−A, following means could be used: (i) enhancing electron-donating capability of donor or π-spacer; (ii) improving acceptors' ability for electron-withdrawn; and (iii) increasing the length of π-bridge.[12,13] With further advancement, Zhang et al.[14] proposed a D−A−π−A structure which combined an auxiliary acceptor, functioning as an electron trap into customary D−π−A organic dyes. It improves their ICT and diminishes the optical band gap. This resulted in red-shifting of the ICT absorption band and facilitates electron transport from D unit to anchor group.[15]

In D−A−π−A organic dyes, D is the electron donor group, first A represents the internal electron acceptor unit followed by conjugated π-spacer and terminal acceptor. Complete experimental analysis followed by deprotonation calculation by Wu et al.[16] proved that the obtained spectral range of D−

Received: November 2, 2018
Revised: December 28, 2018
Published: January 18, 2019

DOI: 10.1021/acs.jpcc.8b10708
J. Phys. Chem. C 2019, 123, 3309−3320

A−π−A structured organic dyes is superior to that of D−π−A ones. This experiment was performed for indoline (IND)-based dye. This dye represents a proficient electron donor with strong electron donating capability.

Other significant characteristics that should be examined thoroughly in order to design efficient DSSCs include the electron-transfer, recombination method, highest occupied molecular orbital (HOMO) and lowest unoccupied molecular orbital (LUMO) shift, band gap offset, and ICT at the interface between the semiconductor TiO_2 and the studied dyes.[17]

IND dyes have been examined as highly efficient sensitizers for DSSCs because of their intense and stable absorption spectra in the visible zone. This makes them one of the potential top-quality chemical classes for future DSSCs with better PCE.[14,16,18−21] In our previous study, we have designed IND dyes explicit to iodine electrolyte based on the developed quantitative structure−property relationship (QSPR) model. Subsequently, we screened all designed dyes based on the essential photophysical parameters with the use of quantum chemical calculations. Our proposed seven lead dyes have D−A−π−A framework and are characterized by the encouraging PCE values.[22] Designed IND dyes consist of an IND moiety that acts as the donor group. Either benzothiadiazole (BTD) or pyrido[3,4-*b*]pyrazine (pyrazine) act as the internal acceptor followed by π spacer and cyanoacrylic acid group as the terminal acceptor.

To expand reported investigations[22] to the next level of screening, in this work additional optoelectronic and interfacial properties of the isolated dyes and dyes bound to TiO_2 cluster, respectively, were examined. Computational approaches were used to calculate different cluster models to gain meaningful explanation of the local properties of the TiO_2.[23,24] For instance, many theoretical studies considered different sizes of cluster models to gain details related to various organic dyes. Phenoxazine and carbazole-based dyes were studied with the use of $(TiO_2)_{16}$[25] and $(TiO_2)_{38}$,[26] respectively. IND dyes were studied in conjunction with $(TiO_2)_{38}$[27] and $(TiO_2)_6$[10] clusters. On the basis of the literature, we modeled our dye@TiO_2 complex using small $(TiO_2)_{16}$ cluster to simulate the TiO_2 (101) surface. Multiscale simulation approaches[28] and non-adiabatic molecular dynamics simulation[27] have been also implemented to study optoelectronic properties of isolated T-shaped organic dyes and IND dyes, respectively.

In this context, computational investigations focused on the density functional theory (DFT) combined with time-dependent DFT (TDDFT) to compute not only electronic structure but also the critical parameters that govern the values of the vital solar cell characteristics: short-circuit current (J_{SC}) and the open-current voltage (V_{OC}) were performed. All critical parameters including light absorption spectra for panchromatic region, electron injection, charge recombination, shift of conduction band (CB) edge, ICT, exciton binding energy, as well as excited state lifetime, and photostability of the dye−cluster complex were computed. Natural population analysis (NPA) was carried out to estimate the amount of CT from dye to Ti atoms of the cluster. Introspection of complete analysis of obtained results suggests that proposed here, new efficient IND dye-sensitizers for DSSCs attain higher photo-to-electron conversion efficiency that could be used for future applications.

MODELS AND COMPUTATIONAL DETAILS

Photo-to-electron conversion efficiency of DSSCs is determined by the following relation[29]

$$\eta = \mathrm{FF}\frac{J_{SC} \times V_{OC}}{P_{IN}} \times 100\% \tag{1}$$

Open-circuit photo voltage (V_{OC}) can be estimated by the following relation in terms of the CB edge (E_C) of semiconductor[30]

$$V_{OC} = \frac{E_{CB}}{q} + \frac{kT}{q}\ln\left(\frac{n_c}{N_{CB}}\right) - \frac{E_{redox}}{q} \tag{2}$$

where E_{redox} is the electrolyte Fermi-level, kT is the thermal energy, q is the unit charge, n_c is the number of electrons in the CB, and N_{CB} is the accessible density of CB states. After dye adsorption on semiconductor, E_{CB} can be expressed as the absolute value of dipole moment of the individual dye molecule perpendicular to the surface of semiconductor surface (μ_{normal}) as given by eq 3.[7]

$$\Delta CB = -\frac{q\mu_{normal}\gamma}{\epsilon_0\epsilon} \tag{3}$$

where q is the electron charge, γ is the dye's surface concentration, ϵ_0 and ϵ are the permittivity of the vacuum and the dielectric constant of the organic monolayer, respectively.

The short circuit current density (J_{SC}) or electron injection efficiency depends on the absorption coefficient of the dye and the interaction between the dye and the nanocrystalline TiO_2 surface. The lifetime τ of the excited state is one of the critical factors to evaluate the efficiency of CT via injection of the excited state electron. A dye with a longer lifetime in the excited state is expected to be more facile for CT. In the present investigation, the τ value is approximately set to the lifetime of spontaneous luminescence, which is evaluated by the following equation[31,32]

$$\tau = \frac{1}{A_{k,k'}} \tag{4}$$

$$A_{k,k'} = \frac{4e^2\Delta E_{k',k}{}^3}{3\hbar^4c^2}|r_{k,k'}|^2 \tag{5}$$

where $A_{k,k'}$ is the Einstein coefficient for spontaneous emission, e is the elementary charge, c is the speed of light in a vacuum, and $\hbar\left(=\frac{\text{Planck's constant, } h}{2\pi}\right)$ is the reduced Planck's constant. Moreover, $\Delta E_{k',k}$ and $r_{k,k'}$ represent the transition energy and transition dipole moment from k to k′ state, respectively. Furthermore, all designed dyes had been checked based on the Marcus theory[33] by calculations of the CT rate using the following equation

$$k_{ET} = \frac{1}{\sqrt{\lambda_{total}}}\sqrt{\frac{\pi}{\hbar^2k_BT}}|V^2|\exp\left\{-\frac{\lambda_{total}}{4k_BT}\right\} \tag{6}$$

In eq 6, except reorganization energy, λ_{total}, all the parameters on the right-hand side are constant. Thus, electron transfer rate constant (k_{ET}) depends only on λ_{total}, which is the sum of hole reorganization (λ_h) and electron reorganization (λ_e) energy, whose values can be estimated by eqs 7[34] and 8, respectively.

DOI: 10.1021/acs.jpcc.8b10708
J. Phys. Chem. C 2019, 123, 3309−3320

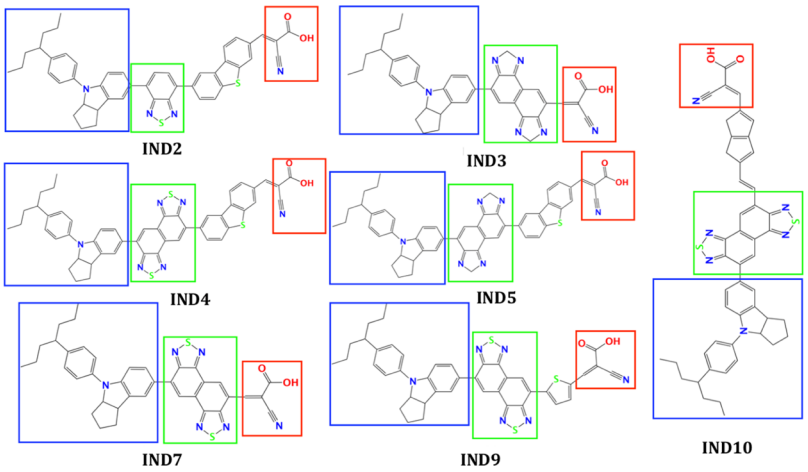

Figure 1. Chemical structures of studied seven IND dye-sensitizers with D−A−π−A framework. Colored boxes are indicating constituents of the framework. Blue (D), green (A or internal acceptor), red (A or cyanoacrylic acid), and the fragment in between red and green box is the π-spacer.

$$\lambda_h = (E_0^+ - E_+^+) + (E_+^0 - E_0^0) \quad (7)$$

$$\lambda_e = (E_0^- - E_-^-) + (E_-^0 - E_0^0) \quad (8)$$

where $E_0^+(E_0^-)$ denotes the energy of cation (anion) calculated from the optimized structure of the neutral molecule; $E_+^+(E_-^-)$ is the energy of cation (anion) calculated from the optimized cation (anion) geometry; $E_+^0(E_-^0)$ is the energy of neutral molecule computed from the cationic (anionic) state; and E_0^0 is the energy of neutral molecule at the ground state.

All IND dyes designed by us are depicted in Figure 1. Both the ground state and excited state calculations were performed using Gaussian09 package.[35] Ground state optimization of designed dyes and dyes bound to the TiO_2 cluster was carried out using B3LYP hybrid functional with 6-31g(d,p) for C, N, O, and S atoms, while effective core potential LANL2DZ and its corresponding basis set were used for Ti and I atoms. Coulomb attenuating CAM-B3LYP functional including long-range correction was chosen to calculate the vertical excitation energies and the oscillator strengths (OSs) within the TD-DFT framework with the abovementioned basis sets, as it is considered to be one of the best methods to predict reasonable excitation energies and the absorption spectra.[22,36,37] We have incorporated solvent effects in both DFT and TDDFT levels of theory using the conductor-like polarizable continuum (C-PCM) model[38] with acetonitrile (AN) solvent as it is one of the most common solvent used in DSSCs fabrication. The TDDFT single-point calculations were performed with the solvent phase DFT optimized geometry. To obtain vertical excitation energies and OSs of the dyes and dyes bound to the TiO_2 cluster, lowest 10 singlet−singlet transitions of the optimized ground state geometry in gas and solvent phase were selected. The dipole moments of the free dyes were also obtained at the geometry of the dyes bound to TiO_2 under the C-PCM-B3LYP/6-31g(d,p) level approach. NPA based on the B3LYP and CAM-B3LYP density matrix has been carried out to confirm the electron injection from the dye to the TiO_2 surface.

Experimental and computational studies have shown three different types of binding of a dye to TiO_2 cluster such as monodentate, chelated and bridged bidentate, the latter one being the most stable.[39−42] To simulate anatase $TiO_2(101)$ surface, a model cluster $[(TiO_2)_{16}(H_2O)_2]$ was constructed by cutting from an anatase (101) surface anatase TiO_2. This latter was built replicating (5, 3, 2) the unit cell by means of the VESTA program, as described elsewhere.[40] This cluster model has been successfully studied for the adsorption of different dyes.[25,40,43,44] Also, the Persson et al.[45] explained that small scale theoretical models of TiO_2 give reasonable results without showing significant discrepancies compared to large models.[46,47] Small clusters such as $(TiO_2)_{16}$ usually give rational outcomes in small-scale theoretical models and exhibited insignificant variances with large and periodic models.[25,40,44,47,48]

RESULTS AND DISCUSSION

Studied IND Dyes and Cluster. Figure 1 displayed the seven IND dyes which were designed based on the QSPR model. The description of the complete procedure can be found in our previous work.[22] All the investigated dyes possess four important constituents: electron donor group (IND derivatives moiety), internal electron acceptor unit (IA), conjugated π-spacer, and cyanoacrylic acid group (terminal acceptor or anchoring moiety). The above-mentioned four constituents generate D−A−π−A family dyes, which differ from the conventional D−π−A architecture of metal-free organic dyes. Recent studies showed that the D−A−π−A molecular framework can be superior to the D−π−A, both in stability and efficiency.[27,49] Often molecular design results in recommending structural changes which may help to enhance different optoelectronic properties of photovoltaics. In this study, designed dyes incorporate internal acceptors units: BTD and pyrazine. Both units are promising candidates to enhance the photovoltaic properties by electron-withdrawing ability in organic polymer solar cells.[50,51] The BTD moiety is increasing the efficiency of charge separation because of its narrow band gap and acts as electron trap.

Figure 2 illustrates the details of the TiO_2 cluster along with the optimized structure of IND2@cluster. The rest of the dye@cluster optimized structures are reported in Figure S1 (see Supporting Information). We have employed two different methods (B3LYP & CAM-B3LYP) for the ground state geometry optimization of the small TiO_2 cluster, $(Ti_{16}O_{34}H_4)$. We performed all calculations with fully relaxed TiO_2 cluster model because chemical bond energy has a significant influence on adsorption energy. Computed orbital energies at the B3LYP level are −8.7652 and −3.5346 eV for

DOI: 10.1021/acs.jpcc.8b10708
J. Phys. Chem. C 2019, 123, 3309−3320

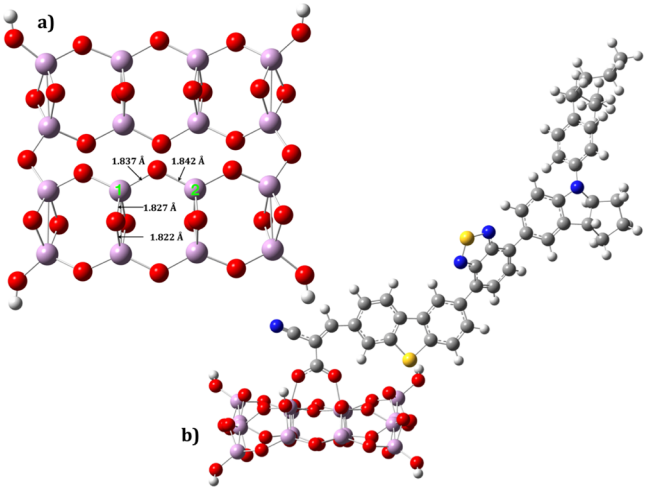

Figure 2. Optimized geometry of the model TiO_2 cluster with important bond lengths (in Å) and the IND2@cluster with bridged bidentate mode. Color code: pink (titanium), red (oxygen), gray (carbon). Yellow (sulfur), blue (nitrogen), and white (hydrogen).

HOMO and LUMO frontier orbitals, respectively. The HOMO−LUMO gap, 5.23 eV, is aligned with the reported value of 5.10 eV[45] and the LUMO energy level is also near to the CB energy of TiO_2 reported experimentally.[52] On the other hand, the corresponding CAM-B3LYP level energies are −10.2721 and −2.4485 eV. Hence, the size of the cluster is sufficient to approximate the bulk TiO_2.

Energetics of Isolated Dyes and Dyes Bounded to Cluster. For the efficient electron injection from the sensitizer to CB of TiO_2, HOMO level or ground state oxidation potential (GSOP) must be lower than the redox potential. The LUMO or excited state oxidation potential (ESOP) should be higher than the CB of TiO_2. In our previous study, we showed that the investigated dyes are satisfying all the prerequisites of the photo efficient DSSCs.[22] All the dyes are adsorbed on the TiO_2(101) surface in bridged bidentate mode and the adsorption energies (ΔE_{ads}) for all of the adsorbed systems are computed by the equation: ($\Delta E_{ads} = E_{dye@TiO_2} - E_{dye} - E_{TiO_2}$). The two oxygen atoms are covalently bonded with two Ti atoms of the TiO_2 cluster. Table 1 displays the adsorption energy and the average bond lengths of surface Ti atom and O atom of the −COOH group along with C−O bond in −COOH group after adsorption. The calculated average Ti−O distances in all the dye−TiO_2 complexes are in the range within 2.00−2.04 Å, which is comparable to the Ti−O bond-length in the bulk TiO_2 (1.934−1.980 Å), confirming that chemisorption of the dyes on the TiO_2(101) surface occurs. The strong chemical bonding between the dyes and TiO_2(101) facilitates the charge injection to the semiconductor. In the present study, we compared the HOMO and LUMO of the dye bounded to TiO_2 cluster. Figure 3a depicts the comparison of the energy levels between a free dye and a dye sensitized TiO_2 form. The data displayed in Figure 3 suggest that the energy gap between the HOMO and LUMO levels decreases when the dye is attached to the TiO_2 cluster. Some reports found that the HOMO level is closely related to the donor, and the LUMO level is mainly affected by the acceptor.[53] When the dyes are adsorbed on the surface of TiO_2 cluster, the LUMO and the TiO_2 film will create relative strong electronic coupling due to the interactions between acceptor group and TiO_2 surface, which lowers the LUMO of original molecules. Comparing the energy level of seven dyes after adsorption, one concludes that LUMO is increasing in the order: IND3(0.266 eV) < IND10(0.302 eV) < IND7(0.314 eV) < IND9(0.370 eV) < IND5(0.692 eV) < IND2(0.854 eV) < IND4(0.926 eV), and the HOMO decreased from 0.07 eV (IND5) to 0.15 eV (IND10) except IND2 (increase by 0.06 eV) and IND4 (remains almost the same). The energy gap (E_{gap}) between the frontier molecular orbitals (FMOs) after adsorption on the cluster E_{gap} of IND5 (1.16 eV) is the lowest while IND7 (1.80 eV) is the highest one. The dependence of electric properties on the structural attributes of the individual dyes plays an important role in changing the orbital localization and in facilitation of electron transport.[54,55]

Table 1. Adsorption Energy (in eV) of IND Dyes on the TiO_2 Cluster[a]

		average bond length (Å)	
name	adsorption Energy (eV)	d_{Ti-O^-}	$d_{C-\bar{O}}$
IND2	−1.049	2.04	1.28
IND3	−1.423	2.00	1.28
IND4	−0.863	2.01	1.28
IND5	−0.958	2.00	1.28
IND7	−0.998	2.03	1.28
IND9	−0.910	2.03	1.28
IND10	−0.993	2.01	1.28

[a]Average bond length (in Å) of bonded Ti atoms and O of the −COOH groups of dyes along with the C and O atoms of −COOH group after adsorption.

UV−Vis Spectra in Solution. *Isolated Dyes.* The characteristic of light absorption of any dye is one of the most important factors to consider in order to increase the efficiency of J_{SC}, according to the equation: $J_{SC} = \int LHE(\lambda)\Phi_{inject}\eta_{collect}\, d\lambda$. Absorption spectra of the designed dyes and dyes bound to TiO_2 cluster are shown in Figure 3. Table 2 shows the absorption wavelength, OS, and initial and excited state orbital contributions. Figure 3b suggests that the absorption spectra of dyes reveal a good response to the solar spectrum and all the dyes (except IND2 and IND4) cover almost the whole visible and even part of infrared light region. Also, the absorption spectra of all the dyes show the double-peak characteristics with a significant separation between two dominant peaks. Among the two peaks, the peak around ≤330 nm might originate from localized $\pi \rightarrow \pi^*$ excitation of IND unit,[16] while the higher wavelength peak is probably attributed to the ICT from the donor (IND derivatives) to acceptor (cyanoacrylic acid) via internal acceptors unit in a HOMO to LUMO transition. If one compares the dye structures (Figure 1), it is obvious that the addition of two internal acceptor units in fused form enhances the photon harvesting efficiency by extending the absorption spectra to infrared region. Again, if one compares the position of ICT bands of the isolated dyes, IND3 and IND5 are characterized by relatively higher wavelength due to the presence of pyrazine unit. Except for IND2, the transition related to the highest energy band is mainly from HOMO to LUMO. The highest energy transition of IND2 is HOMO to LUMO + 1, while the HOMO to LUMO transition for this dye can be described as $S_0 \rightarrow S_4$. FMOs such as HOMO and LUMO are crucial for the electron injection and dye regeneration. Figure 4 displays important FMOs of the

DOI: 10.1021/acs.jpcc.8b10708
J. Phys. Chem. C 2019, 123, 3309−3320

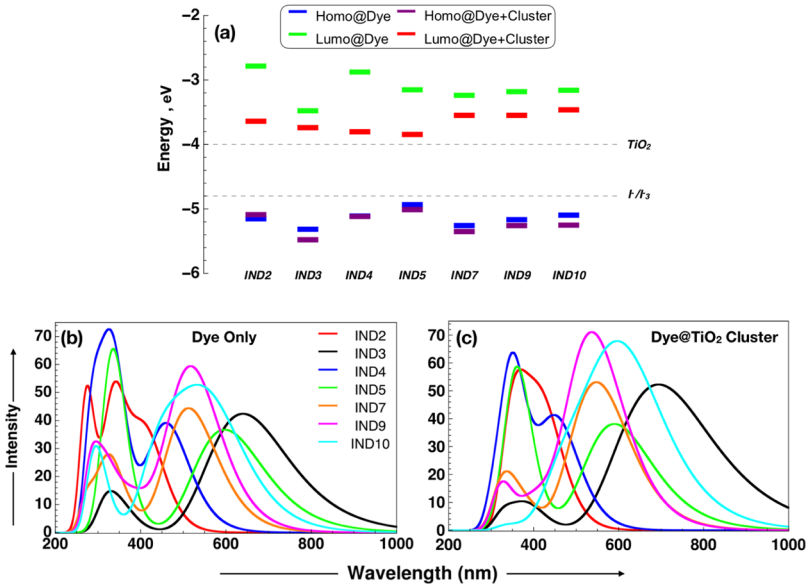

Figure 3. (a) Schematic energy level diagram of the isolated IND dye-sensitizers and adsorbed dye@cluster complex along with the CB of TiO_2 and I^-/I_3^- redox potential. (b) Simulated UV−vis absorption peak of dye and (c) dyes bound to TiO_2 cluster in AN solvent at C-PCM/CAM-B3LYP/6-31G(d,p) level of theory with the B3LYP/6-31G(d,p) optimized geometry with the lowest 10 singlets. For Ti only LANL2DZ basis set was used.

designed isolated dyes. For all the cases, HOMO is concentrated on the donor moiety IND units and spreads over π-spacer. The position of LUMO can be categorized in two classes: (i) it is concentrated on internal acceptor units (in IND2 and IND4), and (ii) it is distributed on the cyanoacrylic acid groups and π-spacer including internal acceptor units. The above analysis of the simulated spectra confirms that the addition or modification of the internal acceptor units displayed a significant effect on the electron excitation. In addition, the lifetime (τ) of the first excited state can be evaluated by eqs 4 and 5. IND3 is characterized by the longest lifetime due to the relatively lower $\Delta E_{k,k'}$ and $r_{k,k'}$ values in electron injection from dye to semiconductor surface. This is also reflected in the UV−vis spectra Figure 3b. Higher excited states hoping such as HOMO to LUMO + 2, LUMO + 3, and LUMO + 5 contribute to the absorption band and CB region of the isolated dyes and dye bound to the TiO_2 surface.

Dye Adsorbed on the TiO_2 Cluster. All the designed dyes are adsorbed on the TiO_2 cluster via BB mode. In our study, we allow the cluster to fully relax in TD/CAM B3LYP/level of theory in AN solution followed by computing of UV−vis spectra. Summary of the calculations is listed in the Table S1 (see Supporting Information). For the first band, the transition characters of five IND dyes bounded to the TiO_2 cluster are predominantly from the HOMO to LUMO, which are similar to those for free dyes in solution. However, IND2 and IND4 have different transition characteristics. They include the combination of higher-energy LUMOs and their first excited state transitions HOMO to LUMO + 9 and HOMO to LUMO + 3, respectively. Those higher energy transitions limited their absorption nature, which makes it not efficient for harvesting energy from the wide range of visible region. Three different patterns of FMOs of dye@clusters can be observed in the Figure 5: (i) LUMO totally located on the TiO_2 cluster (IND2, IND5, and IND9); (ii) LUMO distributed from the cluster to anchoring group to π-linker of the dye, (IND4); and (iii) LUMO located in the dye, only including anchoring group (IND3, IND7, and IND10). However HOMOs of all dyes are located only in the donor unit and to some extent at π-linker. After inspecting the UV−vis spectra and FMOs, one can suggest that all the dyes are potential candidates for DSSCs, nevertheless with some limitations.

Intramolecular Charge Transfer. Light absorption by the dyes benefits from the transition of ICT and excited states with significant charge separation properties.[56] It might be facilitated by ultrafast interfacial electron injection from the sensitized dye to the CB of TiO_2. Also, such a process could reduce the degree of electron recombination with the oxidized dye. Index of spatial extent method[57,58] is used to describe the ICT process qualitatively. The spatial index like the distance between two barycenters density distribution upon excitation (d_{CT}), transferred charge (q_{CT}), and half of the sum of two centroid axes along the electron transfer direction (H) associated with the TDDFT transitions and quantify the through-space character related to the transitions. Also, the term t can be related to $t = d_{CT} - H$, a reasonable diagnostic index to quantify through space transitions. Considering that CT, for a rod-like systems, occurs along the x axis H can be expressed as[58]

$$H = \frac{\sigma^{+x} + \sigma^{-x}}{2} \tag{9}$$

where σ is the root mean square deviation distance along the x axis. A larger value of t indicates that the separation is large between the density increment and depletion regions. Exciton binding energy (E_b) also affects the ICT process which can be estimated by the energy difference between the electronic and optical band gap ($E_b = \Delta E_{HL} - E_{S1}$),[59,60] where the first term is HOMO−LUMO gap and the second one is the first singlet excitation energy. All the above parameters are tabulated in the Table 3. The q_{CT} and d_{CT} values are more substantial for IND7 with shorter π-linker while for IND10 having longer π-linker with lower values. Most of the dyes (except IND3 and IND7) possess $H > d_{CT}$, which confirms the overlap between centroids

DOI: 10.1021/acs.jpcc.8b10708
J. Phys. Chem. C 2019, 123, 3309−3320

Table 2. Electronic Transition Data of IND Dye-Sensitizers Computed by C-PCM/CAM-B3LYP/6-31G(d,p) in the AN Solution at B3LYP/6-31G(d,p) geometries

		wavelength				
dye	state	E, eV	λ_{abs}, nm	OS, f	transition character	$r_{k,k'}$
IND2	S_1	2.99	414.74	0.8324	H → L + 1 (86.3%)	11.654
	S_2	3.43	361.58	0.1478	H − 1 → L (48.2%)	
	S_3	3.67	337.76	1.1449	H − 2→L (90.8%)	
	S_4	3.99	310.04	0.0128	H → L (50.3%)	
	S_5	4.03	307.95	0.0132	H − 1 → L + 1 (65.3%)	
	S_6	4.50	275.61	0.2678	H − 7 → L + 1 (77.4%)	
	S_7	4.51	274.78	0.8981	H → L + 2 (49.4%)	
	S_8	4.53	273.75	0.0790	H − 2 → L + 1 (39.6%)	
	S_9	4.60	269.65	0.0208	H − 4 → L + 1 (21.0%)	
	S_{10}	4.70	264.26	0.0024	H − 2 → L + 1 (14.1%)	
IND3	S_1	1.94	640.08	1.0478	H → L (89.8%)	22.067
	S_2	3.06	404.78	0.0063	H − 1 → L (86.5%)	
	S_3	3.43	361.83	0.1689	H → L + 1 (72.2%)	
	S_4	3.82	324.97	0.0164	H − 2 → L (69.4%)	
	S_5	3.85	322.37	0.2670	H → L + 2 (69.5%)	
	S_6	3.95	314.09	0.0003	H − 5 → L (53.0%)	
	S_7	4.01	309.44	0.0001	H − 6 → L (32.9%)	
	S_8	4.14	299.37	0.0252	H − 3 → L (73.5%)	
	S_9	4.26	291.05	0.0006	H − 8 → L (34.4%)	
	S_{10}	4.49	276.00	0.0012	H − 9 → L (29.2%)	
IND4	S_1	2.69	460.92	0.9572	H → L (78.0%)	14.5251
	S_2	3.47	357.14	0.2306	H − 1 → L + 1 (44.6%)	
	S_3	3.52	352.60	0.1133	H − 1 → L + 1 (56.0%)	
	S_4	3.70	335.25	1.1182	H − 2 → L + 1 (85.4%)	
	S_5	3.84	322.69	0.0005	H → L + 2 (59.3%)	
	S_6	3.97	312.26	0.3789	H − 5 → L (73.8%)	
	S_7	4.02	308.51	0.0414	H → L + 1 (71.6%)	
	S_8	4.27	290.41	0.4823	H − 3 → L (25.2%)	
	S_9	4.34	285.99	0.4332	H − 2 → L (41.5%)	
	S_{10}	4.40	281.77	0.1768	H − 3 → L (42.5%)	
IND5	S_1	2.08	597.15	0.9062	H → L (82.7%)	17.8139
	S_2	3.04	407.19	0.0233	H − 1 → L (75.7%)	
	S_3	3.39	366.09	0.1325	H → L + 1 (36.8%)	
	S_4	3.54	350.59	0.0251	H → L + 2 (69.3%)	
	S_5	3.69	336.36	1.3669	H − 2 → L + 1 (83.6%)	
	S_6	3.82	324.24	0.0243	H → L + 1 (56.6%)	
	S_7	3.88	319.68	0.1052	H − 3 → L (46.7%)	
	S_8	4.01	309.56	0.0350	H − 2 → L (23.0%)	
	S_9	4.02	308.84	0.0246	H − 10 → L (38.3%)	
	S_{10}	4.11	301.52	0.0480	H − 9 → L (33.3%)	
IND7	S_1	2.42	512.62	1.0960	H → L (81.6%)	28.4956
	S_2	3.36	360.52	0.1411	H − 1 → L (67.2%)	
	S_3	3.68	337.00	0.1957	H → L + 1 (41.7%)	
	S_4	3.77	328.84	0.2508	H − 4 → L (49.3%)	
	S_5	4.01	309.48	0.2688	H → L + 2 (55.1%)	
	S_6	4.22	293.83	0.0009	H − 5 → L (38.1%)	
	S_7	4.42	280.66	0.0219	H − 6 → L (35.3%)	
	S_8	4.50	275.70	0.2502	H → L + 3 (46.0%)	
	S_9	4.57	271.06	0.0011	H − 8 → L (65.0%)	
	S_{10}	4.62	268.29	0.0649	H − 1 → L (38.1%)	
IND9	S_1	2.39	518.23	1.4579	H → L (73.0%)	24.8724
	S_2	3.13	396.33	0.2533	H − 1 → L (58.2%)	
	S_3	3.47	357.52	0.1367	H → L + 1 (35.0%)	
	S_4	3.73	331.75	0.0836	H → L + 2 (64.6%)	
	S_5	3.86	320.86	0.4003	H − 4 → L (74.0%)	
	S_6	4.09	302.98	0.0010	H − 2 → L (39.1%)	
	S_7	4.24	292.32	0.0757	H − 6 → L (49.5%)	
	S_8	4.32	287.02	0.1489	H − 6 → L (23.8%)	

DOI: 10.1021/acs.jpcc.8b10708
J. Phys. Chem. C 2019, 123, 3309−3320

Table 2. continued

dye	state	wavelength		OS, f	transition character	$r_{k,k'}$
		E, eV	λ_{abs}, nm			
	S_9	4.34	285.83	0.1213	H − 3 → L (42.6%)	
	S_{10}	4.37	283.55	0.3132	H → L + 3 (22.3%)	
IND10	S_1	2.20	564.48	1.0774	H → L (77.3%)	20.0221
	S_2	2.69	459.68	0.7563	H − 1 → L (38.4%)	
	S_3	2.97	417.62	0.1713	H − 1 → L (43.7%)	
	S_4	3.46	357.94	0.0068	H − 2 → L (62.9%)	
	S_5	3.63	341.85	0.0187	H → L + 2 (45.4%)	
	S_6	3.82	324.94	0.1068	H − 1 → L + 1 (24.7%)	
	S_7	4.07	304.31	0.2008	H − 7 → L (34.4%)	
	S_8	4.11	301.78	0.0236	H − 9 → L (43.9%)	
	S_9	4.26	290.99	0.4695	H → L + 3 (34.8%)	
	S_{10}	4.36	284.44	0.0657	H − 1 → L + 2 (21.8%)	

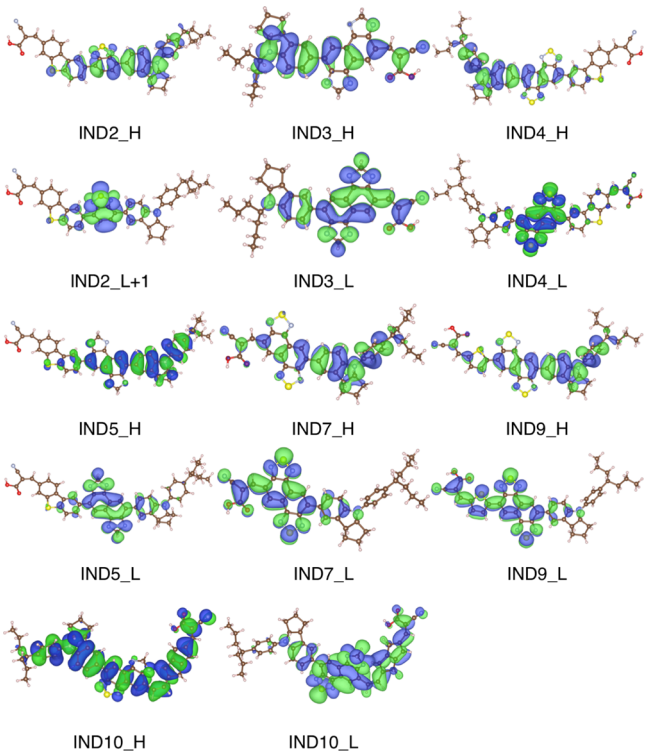

Figure 4. FMOs of the isolated investigated dyes in AN solvent.

along the x axis. Between two internal acceptor units, BTD have larger t values comparing pyrazine. Besides, a larger t value of IND10 indicates large charge separation in the ICT process. Estimated values of d_{CT} and q_{CT} imply that the ICT is more likely to occur in case of IND7 and less likely for IND10. Charge density difference (CDD) of the isolated IND dyes is illustrated in Figure S2 (see Supporting Information). Immediately after ICT, the intramolecular electron−hole pair will be formed. This process is termed as molecular exciton upon photo-excitation. For the propitious separation of the photo-induced exciton, E_b must be overcome and smaller value of E_b efficiently promotes exciton dissociation. Computed values of E_b in Table 3 indicate that the exciton in the dye IND3 is easier to separate compared to other dyes and predicted barrier reaches maximum for IND2. Importantly, all the designed dyes possess lower E_b values than the topmost (maximum % PCE) dye in our IND experimental data set.[22] If one examines the ICT parameter of the dyes adsorbed on the TiO_2 surface (Table 3), it is clear that the charge could be transferred in longer distance to the interface of dyes and semiconductor surface following the increased amount of CT, except the IND5 and IND10 cases.

Photostability of the Designed Dyes. Photostability is one of factors which affect the duration of DSSC devices. To screen the photostability of the designed dyes, we have implemented very fast and robust screening method proposed by De Angelis and coworkers,[46,61] which depends on the aligned excited state energy or ESOP. Aligned level of ESOP is the vital factor that governs the stability of the photo-excited dyes.

Figure 6 depicts the GSOP, ESOP, and the CDDs of $S_0 \rightarrow S_1$. ESOP was computed by the free energy differences of neutral and oxidized molecules in the excited state at the equilibrium geometry of neutral species. ESOP may be approximated by ESOP ≅ GSOP − E_{0-0}, where E_{0-0} is the energy difference between optimized excited and ground states. Because of the large systems considered here, the approximation $E_{0-0} \approx$ vertical excitation energy is applied. We estimated GSOP by the approximation GSOP = $[E_{neutral} - E_{cation}]_{GS}$ and finally ESOP was computed by adding the absorption energy (E_{abs}) to the GSOP. After the analysis of the data of the Figure 6, it is clear that IND2 has high driving force for electron injection to the CB of TiO_2. On the other hand, IND3 has relatively smaller gradient for electron injection which confirms that it is relative photostable among the designed dyes. Moreover, CDD plot of the complex in Figure 6 indicates that IND3, IND7, IND9, and IND10 accumulate charge at the interface. Charge accumulation at the interface favors the continuous electron injection from dye to the surface with the formation of built in electric field.[9] These results support the conclusion of the previous discussions concerning the excited state lifetime based on eqs 4 and 5, as well as the ICT discussions.

Electron Injection. Table 3 displays the optoelectronic properties of the dyes. In DSSCs, electron injection phenomenon can be elucidated by the CT process and Marcus theory can be employed to study the CT process.[33] CT has been associated with the electron injection rate (Φ_{inject}) or efficiency, which may be quantified by the free energy change for electron injection (ΔG_{inject}) in DSSCs, as described in the equation: $J_{SC} = \int \mathrm{LHE}(\lambda)\Phi_{inject}\eta_{collect}\,\mathrm{d}\lambda$. The injection energy can be calculated as[62] $\Delta G_{inject} = E^*_{dye} - E_{CB}$, where E_{CB} is the reduction potential of the CB of the TiO_2 cluster, $Ti_{16}O_{34}H_4$. E_{CB} corresponds to the LUMO energy, (−3.53 eV), of the

DOI: 10.1021/acs.jpcc.8b10708
J. Phys. Chem. C 2019, 123, 3309−3320

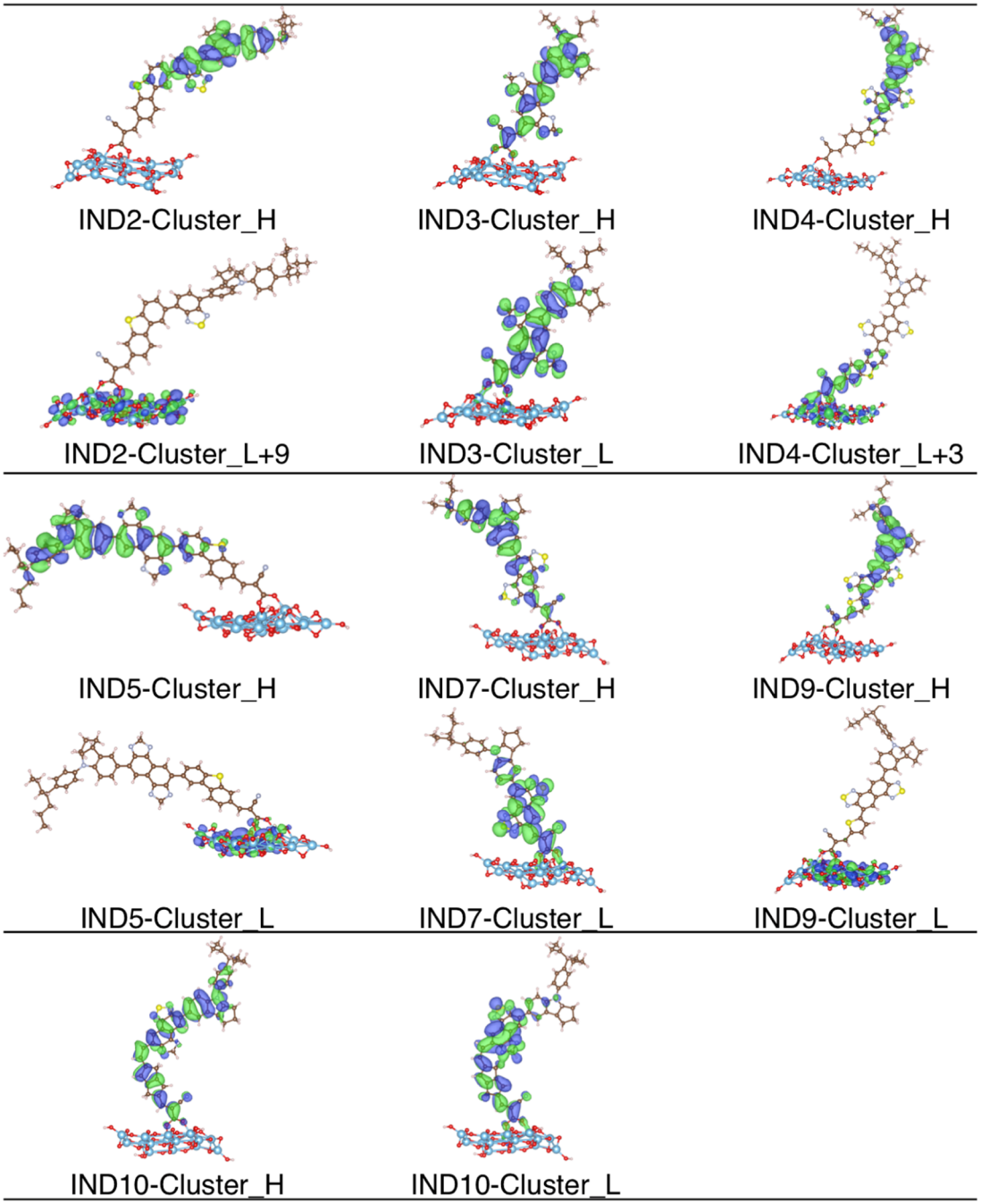

Figure 5. Important molecular orbitals of the IND dyes on the TiO_2 cluster in AN solvent.

Table 3. Computed CT Parameters (d_{CT} in Å and q_{CT} in $|e^-|$) in AN Solvent with TD CAM-B3LYP/6-31g(d,p) Level of Theory[a]

name	E_{dye*}	ΔG_{inject}	λ_h	λ_e	λ_{total}	$E_{\Delta CB}$	μ_{normal}	q_{CT} (e^-)	d_{CT} (Å)	H (Å)	t (Å)	E_b (eV)
IND2	0.628	−2.902	0.36	0.21	0.57	0.42	10.12	0.719 (0.729)	2.937 (3.252)	3.636	0.699	0.64
IND3	1.376	−2.154	0.30	0.27	0.57	0.45	16.26	0.718 (0.744)	4.256 (4.352)	4.053	0.203	0.27
IND4	1.123	−2.407	0.26	0.16	0.42	0.40	5.48	0.724 (0.728)	3.294 (3.436)	4.093	0.799	0.42
IND5	1.098	−2.432	0.18	0.19	0.37	0.25	13.81	0.714 (0.704)	3.661 (3.578)	4.052	0.392	0.34
IND7	1.011	−2.519	0.24	0.25	0.49	0.42	9.96	0.809 (0.847)	4.952 (5.175)	4.353	0.599	0.52
IND9	1.046	−2.484	0.23	0.24	0.47	0.42	8.47	0.664 (0.693)	4.108 (4.577)	5.068	0.960	0.47
IND10	1.238	−2.292	0.36	0.38	0.74	0.48	7.23	0.580 (0.518)	0.655 (0.986)	4.935	4.280	0.29
MAX	2.489	−1.041	0.12	0.01	0.13			0.666	2.647	4.523	1.876	0.91

[a]CB energy of the TiO_2 cluster is the LUMO energy level and it is −3.53 eV.

DOI: 10.1021/acs.jpcc.8b10708
J. Phys. Chem. C 2019, 123, 3309−3320

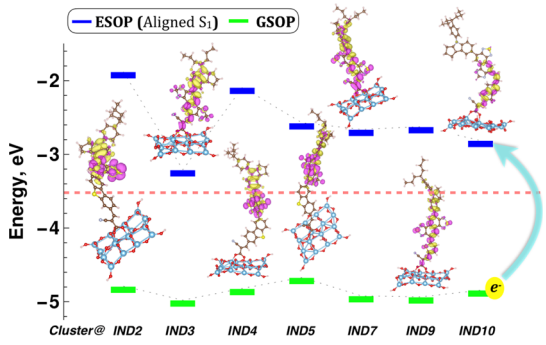

Figure 6. Energy alignment of the IND dyes on TiO_2 along with the CDD of the dyes@cluster complex and CB of TiO_2. Magenta (yellow) indicates positive and negative region with the isovalue of 0.0009 e/Å^3.

cluster. The oxidation potential of the excitation of the dye (E^*_{dye}) can be computed by subtracting the vertical transition energy (λ_{max}) from the redox potential of the ground state of the dye (E_{dye}), whereas $E_{dye} = -E_{HOMO}$, according to Koopmans' theorem. All the designed dyes show the negative values of ΔG_{inject}, which implies that the excited states of the dyes lie above the CB edge of TiO_2 with an effective CT excitation character.[43] The trend of indirect values of J_{SC} is as follows: IND2 (−2.91 eV) > IND7 (−2.52 eV) > IND9 (−2.48 eV) > IND5 (−2.43 eV) > IND4 (−2.41 eV) > IND10 (−2.29 eV) > IND3 (−2.15 eV). This trend might be explained by the property of functional groups involved in their structures: the number of internal acceptor units and the length of π-spacer. We also evaluated the nature of Fermi level shift after the adsorption of different dyes on the TiO2 cluster (in Supporting Information Figure S5). It provides clear evidence that adsorbed dyes introduced new occupied states in the gap region of the TiO_2 cluster, which shift the Fermi or HOMO energy toward the CB edge to facilitate the electron injection.

All the photophysical parameters are tabulated in Table 3. Reorganization energy λ_{total} indicates that the IND5 has the lowest value which suggests the highest ICT rate based on the semiclassical Marcus theory. Also, the value of E_{gap} of IND5 is the lowest before and after adsorption. For the better CT, there should be a balance between the λ_h and λ_e to ensure the transport efficiency of electron from dye to CB of TiO_2 surface. The differences between λ_h and λ_e for all the designed dyes are less than 0.03 eV, except IND2 (0.15 eV) and IND4 (0.10 eV).

Open Circuit Voltage. V_{OC} is one of the salient features of DSSCs, which can be estimated by the eq 3. The shift of the CB of TiO_2 after dye adsorption can be determined qualitatively. Besides, shifting of CB is related to the μ_{normal} of the dyes[7] and synergistic effect of two factors will lead to an increase in V_{OC}, for a defined redox shuttle in DSSCs.[63,64] The larger the μ_{normal} of the adsorbed dye molecules, the higher is V_{OC} value. Here, we estimated the V_{OC} of the designed dyes by quantifying the three main factors: (i) by CB difference, (ii) μ_{normal} of the adsorbed dyes, and (iii) charge distribution of bonded Ti & O atoms evaluated with the help of NPA. Figure 7a represents the partial density of state (PDOS) profiles of the TiO_2 before and after adsorption of IND2 with the linear fittings of the straight portion of that of sigmoid curves. The difference of the CB edge energy ($E_{\Delta CB}$) of the IND2 is measured approximately with the difference of the fitted intercept line with the energy axis. All dyes (see Figure S3 in

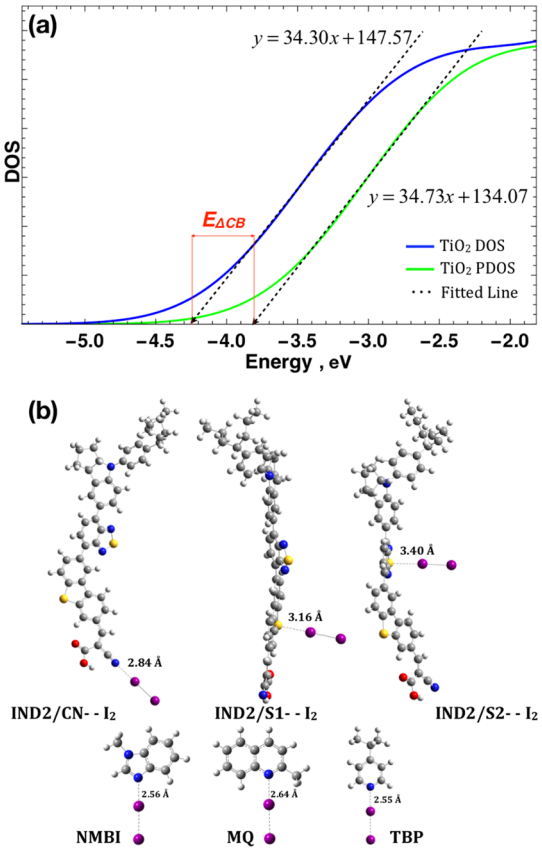

Figure 7. (a) DOS of pristine TiO_2 and PDOS of TiO_2 in the IND2@TiO_2 complex along with the fitted line for the straight portion of the DOS/PDOS. $E_{\Delta CB}$ is the CB shift of TiO_2 after adsorption. (b) Dye−I_2 complex of IND2 with the bond distances of I_2 with the three additives. NMBI: NMN-methylbenzimidazole, MQ: 2-methylquinoline, and TBP: 4-*t*-butylpyridine. Color code: violet (iodine), red (oxygen), gray (carbon). Yellow (sulfur), blue (nitrogen), and white (hydrogen).

see Supporting Information) after adsorption on the TiO_2 surface shift the CB edge of TiO_2 toward the more positive direction with respect to pristine CB of TiO_2. The $E_{\Delta CB}$ provides the indirect evidence that allows us to predict the V_{OC} for the fast screening of newly designed dyes. On the basis of eqs 2 and 3, all the dyes have the same (∼0.4 eV) values of V_{OC}, except IND5 (0.25 eV). The trend of CB shift is as follows: IND10 (0.48 eV) > IND3 (0.45 eV) > IND2 = IND7 = IND9 (0.42 eV) > IND4 (0.40 eV) > IND5 (0.25 eV). We have computed μ_{normal} of the dyes with the solvent effect based on the protocol suggested by the Grätzel et al.,[65] considering the C_2 axis of the carboxylate in dye parallel to the *x*-axis and the TiO_2 surface parallel to the *yz*-plane. The trend of this parameter follows: IND3 (16.26) > IND5 (13.48) > IND2 (10.13) > IND7 (9.96) > IND9 (8.47) > IND10 (7.23) > IND4 (5.49). IND3 and IND5 reveal the higher μ_{normal} values and it might be originated from the pyrazine based internal acceptor unit in their structure. Also, we have obtained results from NPA based on the B3LYP density matrix for the dye, TiO_2, and dye@TiO_2 cluster models in the solvent phases. The obtained values indicate that approximately 0.53−0.62 electrons are transferred from mainly carboxylate group of the dyes to the two nearest Ti atoms when binding to the TiO_2 cluster, (see Table S2 Supporting Information). The NPA results show that in case of IND10, electron transfer from dye

DOI: 10.1021/acs.jpcc.8b10708
J. Phys. Chem. C 2019, 123, 3309−3320

to TiO_2 surface is the highest (0.62 e), while for IND4 is the lowest (0.53 e). The larger $E_{\Delta CB}$, μ_{normal} and n_c values suggest that IND3 and IND10 should be characterized by increased V_{OC} and hence enhanced PCE of DSSCs.

However, the above-estimated values do not guarantee the higher V_{OC} unless the electron recombination reaction can be reduced. Electron recombination might occur by: (i) the iodine electrolytes and (ii) the oxidized dyes.[66] It is well known that electron recombination with electrolyte is dominated by the free iodine concentration and I_2 non-covalently binds with the heteroatoms (such as O, N, S, etc.) of dye.[67] Three major configurations are assumed to model the dye−I_2 interaction and these are (a) I_2 (I_A−I_B) binds with the N of CN moiety; (b) S atom of thiophene ring (S_1) near acceptor units binds with I_2 (I_C−I_D) atom; and (c) S atom of thiophene ring (S_2) far from acceptor units binds with I_2 (I_E−I_F) atom. The optimized structures of dye···I_2 complexes for IND2 are depicted in Figure 7b (see Figure S4 for all other dyes in see Supporting Information) while the bond lengths of I−X (X = I, N, S) are listed in Table S3. In dye···I_2 complex, intramolecular I−I bond lengths are larger than the covalent radii (2.86 Å). This implies that the iodine dimers are weekly bound and the distance of CN and iodine (CN···I_A) atom is smaller than the net van der Waals radii 3.53 Å but larger than the net covalent radii 2.03 Å. Also, the bond lengths between thiophene S and iodine (S···$I_{C/E}$) are larger than the covalent radii, while smaller than the net van der Waals radii (3.78 Å) of the binding atoms. Our previous study also confirms this phenomenon.[9] The additives used to reduce the iodine concentration in the vicinity of TiO_2 are *N*-methylbenzimidazole (NMBI), 2-methylquinoline (MQ), and 4-*t*-butylpyridine (TBP). The bond distances of the optimized additive···I_2 adducts are 2.56, 2.64, and 2.55 Å, respectively, which are smaller than that of the dye···I_2 complexes, indicating that the designed dyes sufficient to reduce the iodine concentration near the TiO_2 surface.

CONCLUSIONS

In summary, we performed a systematic theoretical study of the designed IND-based dyes with DFT and TDDFT methods to evaluate and rationalize their different photophysical parameters which affect the PCE of DSSCs. Effects of structural modification via molecular design on different photophysical properties should balance optimal J_{SC} and V_{OC} values. The various key parameters associated with the V_{OC} and J_{SC} such as vertical dipole moment (μ_{normal}), shift of the CB of semiconductor (ΔE_{CB}), excited state lifetime (τ), driving force of electron injection (ΔG_{inject}), and exciton binding energy (E_b) were computed, and NPA-based analysis was conducted. Because of the widened optical absorption, longer excited state lifetime, highest photostability, highest vertical dipole moment, and lowest exciton binding energy, IND3 would exhibit the better optical and electrical properties than the other considered dyes. The presence of pyrazine-based internal acceptor unit in IND3 is responsible for the enhancement of abovementioned properties. On the basis of the Marcus theory calculation, the ability of hole transfer of IND5, IND7, IND9, and IND10 would be higher than the electron transfer arising from their lower hole reorganization energies, whereas IND5 is the best candidate for ICT with the lowest reorganization energy (λ_{total}). Also, the optical gap of IND5 would leverage higher values of J_{SC}. The NPA and CT analysis confirmed that all designed dyes are capable to inject electrons to the CB of TiO_2. IND10 and IND3 would have benefitted from the shift of CB of TiO_2 by increasing the V_{OC}. Considering the balance between the V_{OC} and J_{SC}, it is obvious that IND3, IND5, and IND10 represent the best potential candidates for the photo efficient DSSCs. The obtained results proved that the rational molecular design provides valuable reference for the synthesis of dyes with higher efficiency.

ASSOCIATED CONTENT

Supporting Information

The Supporting Information is available free of charge on the ACS Publications website at DOI: 10.1021/acs.jpcc.8b10708.

Electronic transition data; NPA results; bond length of the dye−I_2 complex; optimized geometries of the adsorbed dyes@TiO_2 cluster with bridged bidentate binding mode; CDDs; DOS of pristine TiO_2 and PDOS of TiO_2; and Fermi energy level shift of all the IND@TiO_2 complexes (PDF)

AUTHOR INFORMATION

Corresponding Author

*E-mail: jerzy@icnanotox.org. Phone: +1 601 979 3723. Fax: +1 601 979 7823.

ORCID

Juganta K. Roy: 0000-0002-3646-5593
Supratik Kar: 0000-0002-9411-2091
Jerzy Leszczynski: 0000-0001-5290-6136

Notes

The authors declare no competing financial interest.

ACKNOWLEDGMENTS

The authors are thankful to the Department of Energy (grant number: DE-SC0018322) and the NSF EPSCoR (grant number: OIA-1757220) for financial support. We also would like to acknowledge the Extreme Science and Engineering Discovery Environment (XSEDE) by National Science Foundation grant number OCI-1053575 and XSEDE award allocation number DMR110088 and DMR110013P for providing state-of-the-art high-performance computing facilities for supporting this research.

REFERENCES

(1) Nazeeruddin, M. K.; Péchy, P.; Renouard, T.; Zakeeruddin, S. M.; Humphry-Baker, R.; Comte, P.; Liska, P.; Cevey, L.; Costa, E.; Shklover, V.; et al. Engineering of Efficient Panchromatic Sensitizers for Nanocrystalline TiO(2)-Based Solar Cells. *J. Am. Chem. Soc.* **2001**, *123*, 1613.

(2) Nazeeruddin, M. K.; De Angelis, F.; Fantacci, S.; Selloni, A.; Viscardi, G.; Liska, P.; Ito, S.; Takeru, B.; Grätzel, M. Combined Experimental and DFT-TDDFT Computational Study of Photoelectrochemical Cell Ruthenium Sensitizers. *J. Am. Chem. Soc.* **2005**, *127*, 16835.

(3) Hagfeldt, A.; Grätzel, M. Molecular Photovoltaics. *Acc. Chem. Res.* **2000**, *33*, 269−277.

(4) Scholz, M.; Flender, O.; Boschloo, G.; Oum, K.; Lenzer, T. Ultrafast Electron and Hole Transfer Dynamics of a Solar Cell Dye Containing Hole Acceptors on Mesoporous TiO2 and Al2O3. *Phys. Chem. Chem. Phys.* **2017**, *19*, 7158−7166.

(5) Listorti, A.; O'Regan, B.; Durrant, J. R. Electron Transfer Dynamics in Dye-Sensitized Solar Cells. *Chem. Mater.* **2011**, *23*, 3381−3399.

DOI: 10.1021/acs.jpcc.8b10708
J. Phys. Chem. C 2019, 123, 3309−3320

(6) Yao, Z.; Zhang, M.; Wu, H.; Yang, L.; Li, R.; Wang, P. Donor/Acceptor Indenoperylene Dye for Highly Efficient Organic Dye-Sensitized Solar Cells. *J. Am. Chem. Soc.* **2015**, *137*, 3799−3802.
(7) Rühle, S.; Greenshtein, M.; Chen, S.-G.; Merson, A.; Pizem, H.; Sukenik, C. S.; Cahen, D.; Zaban, A. Molecular Adjustment of the Electronic Properties of Nanoporous Electrodes in Dye-Sensitized Solar Cells. *J. Phys. Chem. B* **2005**, *109*, 18907−18913.
(8) Li, H.; Chen, M. Structure-Property Relationships for Three Indoline Dyes Used in Dye-Sensitized Solar Cells: TDDFT Study of Visible Absorption and Photoinduced Charge-Transfer Processes. *J. Mol. Model.* **2013**, *19*, 5317−5325.
(9) Roy, J. K.; Kar, S.; Leszczynski, J. Insight into the Optoelectronic Properties of Designed Solar Cells Efficient Tetrahydroquinoline Dye-Sensitizers on TiO2(101) Surface: First Principles Approach. *Sci. Rep.* **2018**, *8*, 10997.
(10) Ding, W.-L.; Wang, D.-M.; Geng, Z.-Y.; Zhao, X.-L.; Yan, Y.-F. Molecular Engineering of Indoline-Based D-A−π-A Organic Sensitizers toward High Efficiency Performance from First-Principles Calculations. *J. Phys. Chem. C* **2013**, *117*, 17382−17398.
(11) Baheti, A.; Thomas, K. R. J.; Li, C.-T.; Lee, C.-P.; Ho, K.-C. Fluorene-Based Sensitizers with a Phenothiazine Donor: Effect of Mode of Donor Tethering on the Performance of Dye-Sensitized Solar Cells. *ACS Appl. Mater. Interfaces* **2015**, *7*, 2249−2262.
(12) Shibayama, N.; Inoue, Y.; Abe, M.; Kajiyama, S.; Ozawa, H.; Miura, H.; Arakawa, H. Novel Near-Infrared Carboxylated 1,3-Indandione Sensitizers for Highly Efficient Flexible Dye-Sensitized Solar Cells. *Chem. Commun.* **2015**, *51*, 12795−12798.
(13) Qian, X.; Zhu, Y.-Z.; Chang, W.-Y.; Song, J.; Pan, B.; Lu, L.; Gao, H.-H.; Zheng, J.-Y. Benzo[*a*]Carbazole-Based Donor−π−Acceptor Type Organic Dyes for Highly Efficient Dye-Sensitized Solar Cells. *ACS Appl. Mater. Interfaces* **2015**, *7*, 9015−9022.
(14) Zhang, W.; Wu, Y.; Zhu, H.; Chai, Q.; Liu, J.; Li, H.; Song, X.; Zhu, W.-H. Rational Molecular Engineering of Indoline-Based D-A-π-A Organic Sensitizers for Long-Wavelength-Responsive Dye-Sensitized Solar Cells. *ACS Appl. Mater. Interfaces* **2015**, *7*, 26802−26810.
(15) Wu, Y.; Zhu, W. Organic sensitizers from D-π-A to D-A-π-A: effect of the internal electron-withdrawing units on molecular absorption, energy levels and photovoltaic performances. *Chem. Soc. Rev.* **2013**, *42*, 2039−2058.
(16) Wu, Y.; Marszalek, M.; Zakeeruddin, S. M.; Zhang, Q.; Tian, H.; Grätzel, M.; Zhu, W. High-conversion-efficiency organic dye-sensitized solar cells: molecular engineering on D-A-π-A featured organic indoline dyes. *Energy Environ. Sci.* **2012**, *5*, 8261.
(17) Cui, Y.; Wu, Y.; Lu, X.; Zhang, X.; Zhou, G.; Miapeh, F. B.; Zhu, W.; Wang, Z.-S. Incorporating Benzotriazole Moiety to Construct D-A−π-A Organic Sensitizers for Solar Cells: Significant Enhancement of Open-Circuit Photovoltage with Long Alkyl Group. *Chem. Mater.* **2011**, *23*, 4394−4401.
(18) Matsui, M.; Aoki, R.; Nishiwaki, D.; Kubota, Y.; Funabiki, K.; Jin, J.; Yoshida, T.; Higashijima, S.; Miura, H. Importance of Fluorescence Lifetimes for Efficient Indoline Dyes in Dye-Sensitized Solar Cells. *RSC Adv.* **2015**, *5*, 57721−57724.
(19) Hara, K.; Sato, T.; Katoh, R.; Furube, A.; Yoshihara, T.; Murai, M.; Kurashige, M.; Ito, S.; Shinpo, A.; Suga, S.; et al. Novel Conjugated Organic Dyes for Efficient Dye-Sensitized Solar Cells. *Adv. Funct. Mater.* **2005**, *15*, 246−252.
(20) Kitamura, T.; Ikeda, M.; Shigaki, K.; Inoue, T.; Anderson, N. A.; Ai, X.; Lian, T.; Yanagida, S. Phenyl-Conjugated Oligoene Sensitizers for TiO_2 Solar Cells. *Chem. Mater.* **2004**, *16*, 1806.
(21) Horiuchi, T.; Miura, H.; Sumioka, K.; Uchida, S. High Efficiency of Dye-Sensitized Solar Cells Based on Metal-Free Indoline Dyes. *J. Am. Chem. Soc.* **2004**, *126*, 12218−12219.
(22) Kar, S.; Roy, J. K.; Leszczynski, J. In Silico Designing of Power Conversion Efficient Organic Lead Dyes for Solar Cells Using Todays Innovative Approaches to Assure Renewable Energy for Future. *npj Comput. Mater.* **2017**, *3*, 22.
(23) Berardo, E.; Kaplan, F.; Bhaskaran-Nair, K.; Shelton, W. A.; van Setten, M. J.; Kowalski, K.; Zwijnenburg, M. A. Benchmarking the Fundamental Electronic Properties of Small TiO_2 Nanoclusters by *GW* and Coupled Cluster Theory Calculations. *J. Chem. Theory Comput.* **2017**, *13*, 3814−3828.
(24) Berardo, E.; Hu, H.-S.; van Dam, H. J. J.; Shevlin, S. A.; Woodley, S. M.; Kowalski, K.; Zwijnenburg, M. A. Describing Excited State Relaxation and Localization in TiO_2 Nanoparticles Using TD-DFT. *J. Chem. Theory Comput.* **2014**, *10*, 5538−5548.
(25) Li, P.; Cui, Y.; Song, C.; Zhang, H. A Systematic Study of Phenoxazine-Based Organic Sensitizers for Solar Cells. *Dyes Pigm.* **2017**, *137*, 12−23.
(26) Fan, W.-J.; Shi, H.; Tan, D.-Z.; Xu, Z.-N.; Yu, N.-K.; Zhao, J.-L. Design of Novel Phenanthrocarbazole Dyes for Efficient Applications in Dye-Sensitized Solar Cells. *Comput. Mater. Sci.* **2018**, *151*, 34−40.
(27) Chiu, C.-C.; Sheng, Y.-C.; Lin, W.-J.; Juwita, R.; Tan, C.-J.; Tsai, H.-H. G. Effects of Internal Electron-Withdrawing Moieties in D-A−π-A Organic Sensitizers on Photophysical Properties for DSSCs: A Computational Study. *ACS Omega* **2018**, *3*, 433−445.
(28) Zhang, W.; Heng, P.; Su, H.; Ren, T.; Wang, L.; Zhang, J. Rational Design of High-Efficiency Organic Dyes in Dye-Sensitized Solar Cells by Multiscale Simulations. *J. Phys. Chem. C* **2018**, *122*, 25219−25228.
(29) Grätzel, M. Recent Advances in Sensitized Mesoscopic Solar Cells. *Acc. Chem. Res.* **2009**, *42*, 1788−1798.
(30) Marinado, T.; Nonomura, K.; Nissfolk, J.; Karlsson, M. K.; Hagberg, D. P.; Sun, L.; Mori, S.; Hagfeldt, A. How the Nature of Triphenylamine-Polyene Dyes in Dye-Sensitized Solar Cells Affects the Open-Circuit Voltage and Electron Lifetimes. *Langmuir* **2009**, *26*, 2592−2598.
(31) Einstein, A. On the Quantum Theory of Radiation. *Phys. Z.* **1917**, *18*, 121−128.
(32) Yang, L.-N.; Sun, Z.-Z.; Chen, S.-L.; Li, Z.-S. The Effects of Various Anchoring Groups on Optical and Electronic Properties of Dyes in Dye-Sensitized Solar Cells. *Dyes Pigm.* **2013**, *99*, 29−35.
(33) Marcus, R. A. Electron Transfer Reactions in Chemistry. Theory and Experiment. *J. Electroanal. Chem.* **1997**, *438*, 251−259.
(34) Hutchison, G. R.; Ratner, M. A.; Marks, T. J. Hopping Transport in Conductive Heterocyclic Oligomers: Reorganization Energies and Substituent Effects. *J. Am. Chem. Soc.* **2005**, *127*, 2339−2350.
(35) Frisch, M. J.; Trucks, G. W.; Schlegel, H. B.; Scuseria, G. E.; Robb, M. A.; Cheeseman, J. R.; Scalmani, G.; Barone, V.; Mennucci, B.; Petersson, G. A.; et al. *Gaussian 09*, Revision E.01; Gussian, Inc.: Wallingford, CT, 2013.
(36) Yanai, T.; Tew, D. P.; Handy, N. C. A new hybrid exchange-correlation functional using the Coulomb-attenuating method (CAM-B3LYP). *Chem. Phys. Lett.* **2004**, *393*, 51−57.
(37) Kar, S.; Roy, J.; Leszczynska, D.; Leszczynski, J. Power Conversion Efficiency of Arylamine Organic Dyes for Dye-Sensitized Solar Cells (DSSCs) Explicit to Cobalt Electrolyte: Understanding the Structural Attributes Using a Direct QSPR Approach. *Computation* **2016**, *5*, 2.
(38) Cossi, M.; Barone, V. Time-Dependent Density Functional Theory for Molecules in Liquid Solutions. *J. Chem. Phys.* **2001**, *115*, 4708.
(39) Nara, M.; Torii, H.; Tasumi, M. Correlation between the Vibrational Frequencies of the Carboxylate Group and the Types of Its Coordination to a Metal Ion: Anab InitioMolecular Orbital Study. *J. Phys. Chem.* **1996**, *100*, 19812−19817.
(40) Paredes-Gil, K.; Mendizabal, F.; Páez-Hernández, D.; Arratia-Pérez, R. Electronic Structure and Optical Properties Calculation of Zn-Porphyrin with N-Annulated Perylene Adsorbed on TiO 2 Model for Dye-Sensitized Solar Cell Applications: A DFT/TD-DFT Study. *Comput. Mater. Sci.* **2017**, *126*, 514−527.
(41) Anselmi, C.; Mosconi, E.; Pastore, M.; Ronca, E.; De Angelis, F. Adsorption of Organic Dyes on TiO2 Surfaces in Dye-Sensitized Solar Cells: Interplay of Theory and Experiment. *Phys. Chem. Chem. Phys.* **2012**, *14*, 15963.
(42) Zheng, J.; Zhang, K.; Fang, Y.; Zuo, Y.; Duan, Y.; Zhuo, Z.; Chen, X.; Yang, W.; Lin, Y.; Wong, M. S.; et al. How to Optimize the Interface between Photosensitizers and TiO2 Nanocrystals with

DOI: 10.1021/acs.jpcc.8b10708
J. Phys. Chem. C 2019, 123, 3309−3320

Molecular Engineering to Enhance Performances of Dye-Sensitized Solar Cells? *ACS Appl. Mater. Interfaces* **2015**, *7*, 25341−25351.
(43) Mendizabal, F.; Mera-Adasme, R.; Xu, W.-H.; Sundholm, D. Electronic and Optical Properties of Metalloporphyrins of Zinc on TiO2 Cluster in Dye-Sensitized Solar-Cells (DSSC). A Quantum Chemistry Study. *RSC Adv.* **2017**, *7*, 42677−42684.
(44) Guo, M.; He, R.; Dai, Y.; Shen, W.; Li, M.; Zhu, C.; Lin, S. H. Electron-Deficient Pyrimidine Adopted in Porphyrin Sensitizers: A Theoretical Interpretation of π-Spacers Leading to Highly Efficient Photo-to-Electric Conversion Performances in Dye-Sensitized Solar Cells. *J. Phys. Chem. C* **2012**, *116*, 9166−9179.
(45) Persson, P.; Gebhardt, J. C. M.; Lunell, S. The Smallest Possible Nanocrystals of Semiionic Oxides. *J. Phys. Chem. B* **2003**, *107*, 3336−3339.
(46) Pastore, M.; Fantacci, S.; De Angelis, F. Modeling Excited States and Alignment of Energy Levels in Dye-Sensitized Solar Cells: Successes, Failures, and Challenges. *J. Phys. Chem. C* **2013**, *117*, 3685−3700.
(47) Liu, Y. F.; Guan, J.; Hu, D.; Du, L.; Sun, H.; Gao, J.; Zhao, J.; Lan, Z. Computational Investigation of Acene-Modified Zinc-Porphyrin Based Sensitizers for Dye-Sensitized Solar Cells. *J. Phys. Chem. C* **2015**, *119*, 8417−8430.
(48) Pastore, M.; Selloni, A.; Fantacci, S.; De Angelis, F. Electronic and Optical Properties of Dye-Sensitized TiO_2 Interfaces. In *First Principles Approaches to Spectroscopic Properties of Complex Materials*; Di Valentin, C., Botti, S., Cococcioni, M., Eds.; Topics in Current Chemistry; Springer: Berlin, Heidelberg, 2014.
(49) Wu, Y.; Zhu, W.-H.; Zakeeruddin, S. M.; Grätzel, M. Insight into D-A−π-A Structured Sensitizers: A Promising Route to Highly Efficient and Stable Dye-Sensitized Solar Cells. *ACS Appl. Mater. Interfaces* **2015**, *7*, 9307−9318.
(50) Li, Y.; Sun, C.; Song, P.; Ma, F.; Kungwan, N.; Sun, M. Physical Insight on Mechanism of Photoinduced Charge Transfer in Multipolar Photoactive Molecules. *Sci. Rep.* **2018**, *8*, 10089.
(51) Velusamy, M.; Thomas, K. R. J.; Lin, J. T.; Hsu, Y.-C.; Ho, K.-C. Organic Dyes Incorporating Low-Band-Gap Chromophores for Dye-Sensitized Solar Cells. *Org. Lett.* **2005**, *7*, 1899−1902.
(52) Scanlon, D. O.; Dunnill, C. W.; Buckeridge, J.; Shevlin, S. A.; Logsdail, A. J.; Woodley, S. M.; Catlow, C. R. A.; Powell, M. J.; Palgrave, R. G.; Parkin, I. P.; et al. Band Alignment of Rutile and Anatase TiO2. *Nat. Mater.* **2013**, *12*, 798−801.
(53) Meng, S.; Ren, J.; Kaxiras, E. Natural Dyes Adsorbed on TiO_2 Nanowire for Photovoltaic Applications: Enhanced Light Absorption and Ultrafast Electron Injection. *Nano Lett.* **2008**, *8*, 3266−3272.
(54) Kakiage, K.; Aoyama, Y.; Yano, T.; Oya, K.; Kyomen, T.; Hanaya, M. Fabrication of a high-performance dye-sensitized solar cell with 12.8% conversion efficiency using organic silyl-anchor dyes. *Chem Commun.* **2015**, *51*, 6315−6317.
(55) Wen, Y.; Wu, W.; Li, Y.; Li, Y.; Qin, T.; Tang, Y.; Wang, L.; Zhang, J. Thieno[2,3-b]Indole-Based Organic Dyes for Dye-Sensitized Solar Cells: Effect of π-Linker on the Performance of Isolated Dye and Interface between Dyes and TiO2. *Org. Electron.* **2016**, *38*, 61−68.
(56) Martsinovich, N.; Troisi, A. Theoretical Studies of Dye-Sensitised Solar Cells: From Electronic Structure to Elementary Processes. *Energy Environ. Sci.* **2011**, *4*, 4473.
(57) Jacquemin, D.; Le Bahers, T.; Adamo, C.; Ciofini, I. What is the "best" atomic charge model to describe through-space charge-transfer excitations? *Phys. Chem. Chem. Phys.* **2012**, *14*, 5383.
(58) Le Bahers, T.; Adamo, C.; Ciofini, I. A Qualitative Index of Spatial Extent in Charge-Transfer Excitations. *J. Chem. Theory Comput.* **2011**, *7*, 2498−2506.
(59) Gregg, B. A. Excitonic Solar Cells. *J. Phys. Chem. B* **2003**, *107*, 4688−4698.
(60) Scholes, G. D.; Rumbles, G. Excitons in Nanoscale Systems: Fundamentals and Applications. *Annual Review of Nano Research*; World Scientific, 2008; Vol. 2, pp 103−157.
(61) De Angelis, F.; Fantacci, S.; Mosconi, E.; Nazeeruddin, M. K.; Grätzel, M. Absorption Spectra and Excited State Energy Levels of the N719 Dye on TiO2 in Dye-Sensitized Solar Cell Models. *J. Phys. Chem. C* **2011**, *115*, 8825−8831.
(62) Katoh, R.; Furube, A. Electron Injection Efficiency in Dye-Sensitized Solar Cells. *J. Photochem. Photobiol., C* **2014**, *20*, 1−16.
(63) Ronca, E.; Pastore, M.; Belpassi, L.; Tarantelli, F.; De Angelis, F. Influence of the Dye Molecular Structure on the TiO_2 Conduction Band in Dye-Sensitized Solar Cells: Disentangling Charge Transfer and Electrostatic Effects. *Energy Environ. Sci.* **2013**, *6*, 183−193.
(64) Dualeh, A.; De Angelis, F.; Fantacci, S.; Moehl, T.; Yi, C.; Kessler, F.; Baranoff, E.; Nazeeruddin, M. K.; Grätzel, M. Influence of Donor Groups of Organic D−π-A Dyes on Open-Circuit Voltage in Solid-State Dye-Sensitized Solar Cells. *J. Phys. Chem. C* **2012**, *116*, 1572−1578.
(65) Chen, P.; Yum, J. H.; De Angelis, F.; Mosconi, E.; Fantacci, S.; Moon, S.-J.; Baker, R. H.; Ko, J.; Nazeeruddin, M. K.; Grätzel, M. High Open-Circuit Voltage Solid-State Dye-Sensitized Solar Cells with Organic Dye. *Nano Lett.* **2009**, *9*, 2487−2492.
(66) Raga, S. R.; Barea, E. M.; Fabregat-Santiago, F. Analysis of the Origin of Open Circuit Voltage in Dye Solar Cells. *J. Phys. Chem. Lett.* **2012**, *3*, 1629−1634.
(67) Richards, C. E.; Anderson, A. Y.; Martiniani, S.; Law, C.; O'Regan, B. C. The Mechanism of Iodine Reduction by TiO2 Electrons and the Kinetics of Recombination in Dye-Sensitized Solar Cells. *J. Phys. Chem. Lett.* **2012**, *3*, 1980−1984.

DOI: 10.1021/acs.jpcc.8b10708
J. Phys. Chem. C 2019, 123, 3309−3320